Monthly Notices of the ROYAL ASTRONOMICAL SOCIETY
MNRAS **461,** 3982–3992 (2016)
Advance Access publication 2016 July 6
doi:10.1093/mnras/stw1607

Dynamics of rotationally fissioned asteroids: non-planar case

L. A. G. Boldrin,[1★] D. J. Scheeres[2] and O. C. Winter[1]
[1] *UNESP – Univ Estadual Paulista, Grupo de Dinâmica Orbital e Planetologia, Guaratinguetá, SP, Brazil*
[2] *Aerospace Engineer Department, University of Colorado, Boulder, CO, USA*

Accepted 2016 July 4. Received 2016 July 3; in original form 2015 October 8

ABSTRACT

The rotational fission of asteroids has been studied previously with simplified models restricted to planar motion. However, the observed physical configuration of contact binaries leads one to conclude that most of them are not in a planar configuration and hence would not be restricted to planar motion once they undergo rotational fission. This motivated a study of the evolution of initially non-planar binaries created by fission. Using a two-ellipsoid model, we performed simulations taking only gravitational interactions between components into account. We simulate 91 different initial inclinations of the equator of the secondary body for 19 different mass ratios. After disruption, the binary system dynamics are chaotic, as predicted from theory. Starting the system in a non-planar configuration leads to a larger energy and enhanced coupling between the rotation state of the smaller fissioned body and the evolving orbital system, and enables re-impact to occur. This leads to differences with previous planar studies, with collisions and secondary spin fission occurring for all mass ratios with inclinations $\theta_0 \geq 40^{\text{o}}$, and mimics a Lidov–Kozai mechanism. Out of 1729 studied cases, we found that ∼14 per cent result in secondary fission, ∼25 per cent result in collisions and ∼6 per cent have lifetimes longer than 200 yr. In Jacobson & Scheeres stable binaries only formed in cases with mass ratios $q < 0.20$. Our results indicate that it should be possible to obtain a stable binary with the same mechanisms for cases with mass ratios larger than this limit, but that the system should start in a non-planar configuration.

Key words: line: formation – celestial mechanics – minor planets, asteroids: general.

1 INTRODUCTION

Many studies have been done to understand the dynamics and origin of such systems since the discovery of the first binary asteroid system, Dactyl orbiting around (243) Ida in 1993 (Chapman et al. 1995). Based on the structure of 'rubble pile' asteroids (a collection of gravitationally bound boulders with a distribution of size scales and very little tensile strength between them), a model for how they can disrupt due to close flybys of a planet was developed. However, close encounters with the planets proved not to be enough for creation of the current population of binary systems (Margot et al. 2002; Walsh & Richardson 2008). Another model for their formation is by increasing their spin rates due to incident and remitted solar photons, known as the Yarkovsky–O'Keefe–Radzievskii–Paddack (YORP) effect. The YORP effect on contact binary asteroids has been studied (Bottke et al. 2002; Merline et al. 2002; Scheeres 2002; Walsh & Richardson 2006). Using a model with an ellipsoid and a sphere in a planar case, Scheeres (2007) studied fission limits (spin limit to occur a fission) and the stability of that kind of system for different initial conditions. After that, the stability of a binary system was analysed using a two-ellipsoid model (Scheeres 2009). Pravec et al. (2010) made a complete study about formation of asteroid pairs through rotation fission. Jacobson & Scheeres (2011) studied the creation of binaries and other observed near-Earth asteroid (NEA) systems, including doubly synchronous binaries, high-e binaries, ternary systems and contact binaries. That study analysed the dynamics of a binary system just after rotational fission. Using a two-ellipsoid model taking into account mutual gravitational interactions and tidal dissipation, they analysed the dynamics for different mass ratios of the system under a planar assumption. The current work follows from these results, but looks at more likely, non-planar initial configurations. This extension is significant, as non-planar cases must take into account the complete rotational motion (rotation, precession and nutation) of each body. Our results are compared with the results obtained by Jacobson & Scheeres (2011).

After rotational fission, the binary system starts its motion with an unstable chaotic dynamics (Scheeres 2009). To stabilize the system it is necessary to decrease the energy of the system. So, if the spin velocity of one of the binary members increases due to dynamical interactions (spin–orbit coupling) and the spin velocity gets to be

★ E-mail: luizboldrin@yahoo.com.br

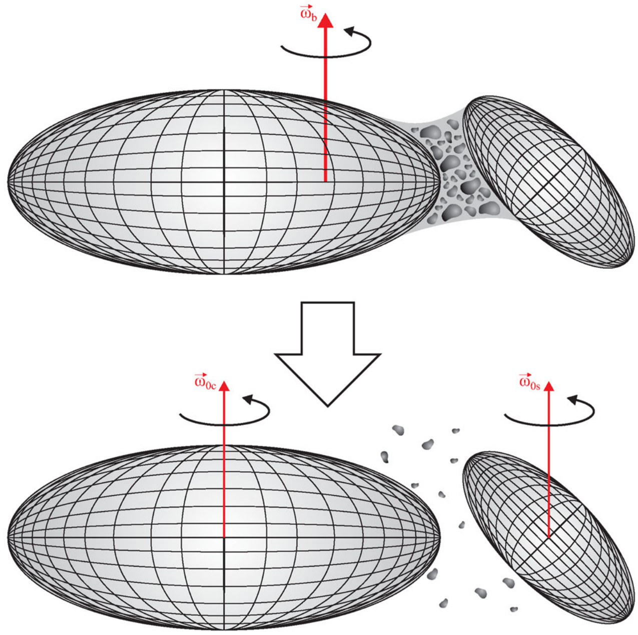

Figure 1. The fission scenario. The contact binary asteroid, composed of two components and some unmodelled small rocks. When the system reaches the spin fission limit the two large components enter orbit about each other and create a binary system.

larger than the spin fission limit, a second fission can occur. The ternary system is also unstable, but the escape of ternary members changes the energy of the system and can stabilize the binary system. Obviously, collisions can also decrease the system energy. Thus, the subject of this work is to study the processes of secondary fission and re-impact, analysing the percentage that occurs in each case.

The paper is organized as follows. Section 2 presents the fission scenario, assumptions and justifications. Section 3 presents the mathematical model based on the physical model adopted. Section 4 considers the dynamical evolution of the system. In Section 5 we present the extreme and final states, analysing the conditions for binary formation. Section 6 provides a summary of our conclusions.

2 FISSION SCENARIO

Rubble pile asteroids are composed of many rocks with different sizes, which have coalesced under the influence of gravity. A contact binary asteroid is composed of two major bodies resting on each other. An asteroid can be both a rubble pile and a contact binary, with an excellent example being Asteroid 25143 Itokawa. The spin rate of such an asteroid can be increased by the YORP effect until it reaches its fission limit and a disruption occur, creating a binary asteroid. Fig. 1 illustrates this with a model of two ellipsoids touching each other with different orientations such that after disruption the bodies have initial obliquities different from zero. These different scenarios yield different system energy and momentum at fission. The energy is higher and the momentum smaller for larger obliquities (θ) resulting in a different behaviour of the orbital and rotational dynamics (see Fig. 2).

3 DYNAMICAL MODEL

We are interested in studying the orbital and rotational evolution of the two large components after its disruption. So, we consider just

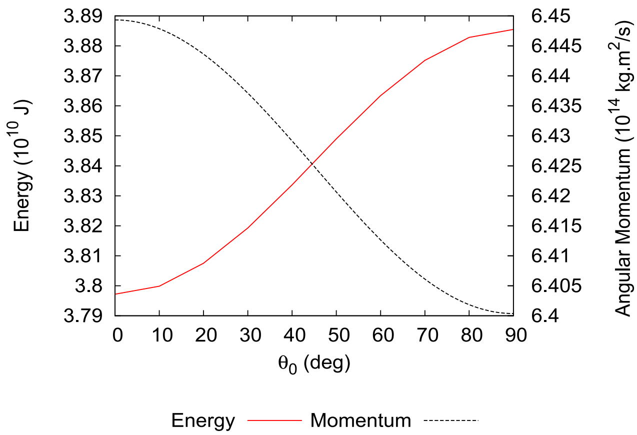

Figure 2. Total energy and magnitude of the total angular momentum of the system as a function of initial Euler angle θ_0. Note that the energy is larger and the momentum is smaller for larger values of θ. Initial conditions: central body with dimensions ($a_{(c)} = 1$ km, $b_{(c)} = 0.7$ km, $c_{(c)} = 0.65$ km); density ($d = 2.0$ g cm^{-3}); mass ratio ($q = 0.1$); initial spin period $T = 5.3586$ h.

gravitational interactions of each other [we do not take into account non-gravitational effects like YORP, binary YORP (BYORP) and tidal dissipation]. This is justified as the short-term dynamics are dominated by the interaction of these bodies. We adopted a model taking into account the translational and rotational motion of two ellipsoids with uniform density. Then, we numerically integrate the equations of motion using the Bulirsch–Stoer method (Press et al. 2007). Fig. 3 shows a scheme of the model with the reference systems and the Euler angles.

3.1 Equations of motion

The equation of the translational motion, using the gravitational potential expressed in terms of spherical harmonics expanded until second order (C_{20} and C_{22}), centred on the centre of mass of one of the bodies (central body), has the common form (Beutler 2005)

$$\ddot{\boldsymbol{r}} = -\mu\frac{\boldsymbol{r}}{r^3} + T_{(c)}^T\nabla' U_2^{(c)} + T_{(s)}^T\nabla' U_2^{(s)}, \tag{1}$$

where $\mu = k^2(M_c + M_s)$, $\boldsymbol{r}$ is the position vector, M_i are the masses of these bodies, k^2 is the gravitational constant, $T_{(i)}$ is the rotational matrix from the inertial system (x, y, z) to the principal axes of inertia (PAI) system (x', y', z'). So, ($'$) means the coordinates are in PAI system and $U_2^{(i)}$ is the gravitational potential (i = c, s for central body and second body, respectively). The gravitational potential is given by

$$U_2^{(i)} = \frac{\mu}{r^3}\left[\frac{C_{20}^{(i)}}{2}\left(\frac{3z'^2}{r^2} - 1\right) + 3C_{22}^{(i)}\left(\frac{x'^2 - y'^2}{r^2}\right)\right]. \tag{2}$$

We consider constant and homogeneous density for both bodies, so we can obtain the gravitational coefficients C_{20} (oblateness) and C_{22} (ellipticity) using the dimensions of the ellipsoid (a, b, c):

$$C_{20}^{(i)} = -\frac{1}{5R^2}\left[c_{(i)}^2 - \frac{\left(a_{(i)}^2 + b_{(i)}^2\right)}{2}\right], \qquad C_{22}^{(i)} = \frac{1}{20R^2}\left(a_{(i)}^2 - b_{(i)}^2\right), \tag{3}$$

where R is the equatorial radius of the ellipsoid. To study the attitude motion, at first we use Euler equations with gravitational torque

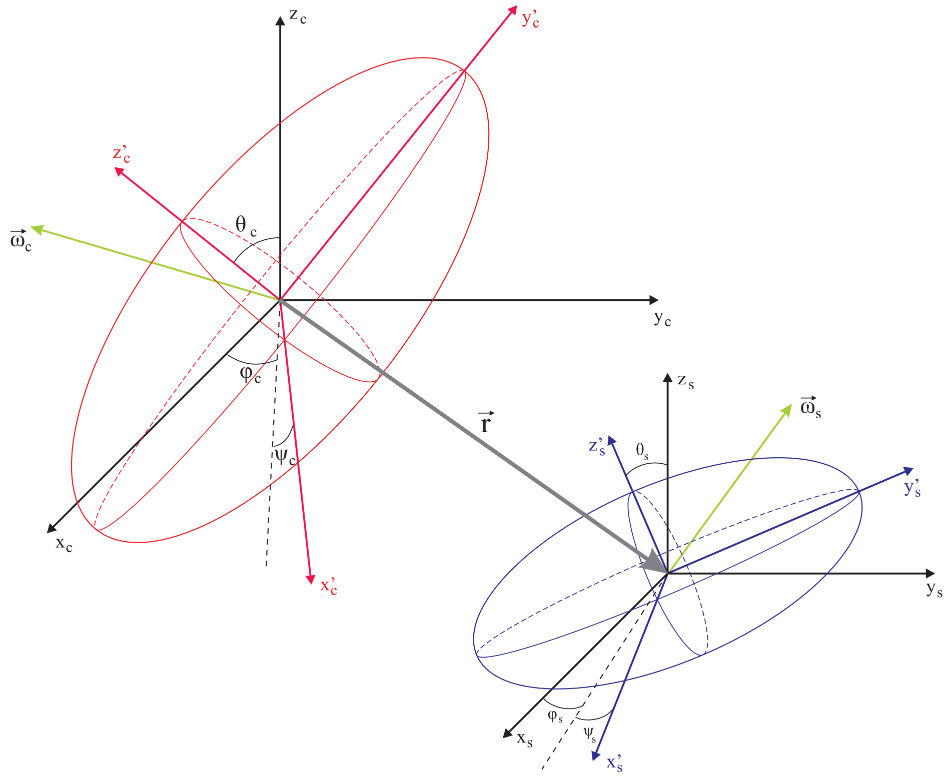

Figure 3. The model that we use. In red is the central body and its PAI system. In blue is the secondary body and its PAI system. The systems ((x_i, y_i, z_i) – i = c, s for central body and second body, respectively) in black we call the inertial system, but these systems are not exactly inertial systems because they are not in the barycentre of the system. Usually that kind of system is the so-called quasi-inertial system because it is not inertial in the translational motion but it is not rotating with respect to any inertial system, so we can use these systems to study the rotational motion using the Euler angles (φ_i, θ_i, ψ_i).

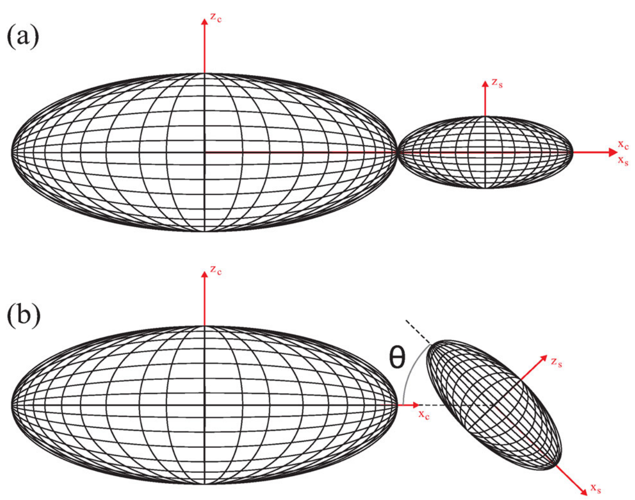

Figure 4. Geometry of the initial conditions. Panel (a) shows the planar case, $\theta = 0$ (Jacobson & Scheeres 2011), and panel (b) shows the non-planar case.

due to another body (a point of mass body) to compute the angular velocity (Beutler 2005):

$$\begin{pmatrix} \dot{\omega}'_x \\ \dot{\omega}'_y \\ \dot{\omega}'_z \end{pmatrix} + \begin{pmatrix} \gamma_1 \omega'_y \omega'_z \\ \gamma_2 \omega'_z \omega'_x \\ \gamma_3 \omega'_x \omega'_y \end{pmatrix} = \frac{3k^2 m_\mathrm{d}}{r_\mathrm{d}^5} \begin{pmatrix} \gamma_1 y'_\mathrm{d} z'_\mathrm{d} \\ \gamma_2 z'_\mathrm{d} x'_\mathrm{d} \\ \gamma_3 x'_\mathrm{d} y'_\mathrm{d} \end{pmatrix}, \tag{4}$$

where m_d is the mass of the disturbing body, r_d is the modulus of the position vector of the disturbing body, (x'_d, y'_d, z'_d) the coordinates of the disturbing body, $\gamma_1 = (C - B)/A$; $\gamma_2 = (A - C)/B$; $\gamma_3 = (B - A)/C$; and A, B and C are the principal moments of inertia of the body, and ω'_x, ω'_y, ω'_z are components of the angular velocity. We note that this model is consistent with the translational model up to second order in the mutual potential.

After obtaining the angular velocity, we can study the rotational motion through the variation of Euler angles. However, the equations of the variation of Euler angles have singularities. So, we decided to use the quaternions (η_1, η_2, η_3, η_4) (Wertz 1978):

$$\dot{\eta}_1 = \frac{1}{2}\left(\eta_4 \omega'_x - \eta_3 \omega'_y + \eta_2 \omega'_z\right), \tag{5}$$

$$\dot{\eta}_2 = \frac{1}{2}\left(\eta_4 \omega'_y - \eta_1 \omega'_z + \eta_3 \omega'_x\right), \tag{6}$$

$$\dot{\eta}_3 = \frac{1}{2}\left(\eta_4 \omega'_z - \eta_2 \omega'_x + \eta_1 \omega'_y\right), \tag{7}$$

$$\dot{\eta}_4 = -\frac{1}{2}\left(\eta_1 \omega'_x + \eta_2 \omega'_y + \eta_3 \omega'_z\right). \tag{8}$$

From the quaternions we can obtain the Euler angles and consequently study the rotational motion of the body.

Note that the equations of the rotational motion (equations 4–8) are just for one body, so we need two sets of equations, one for each body.

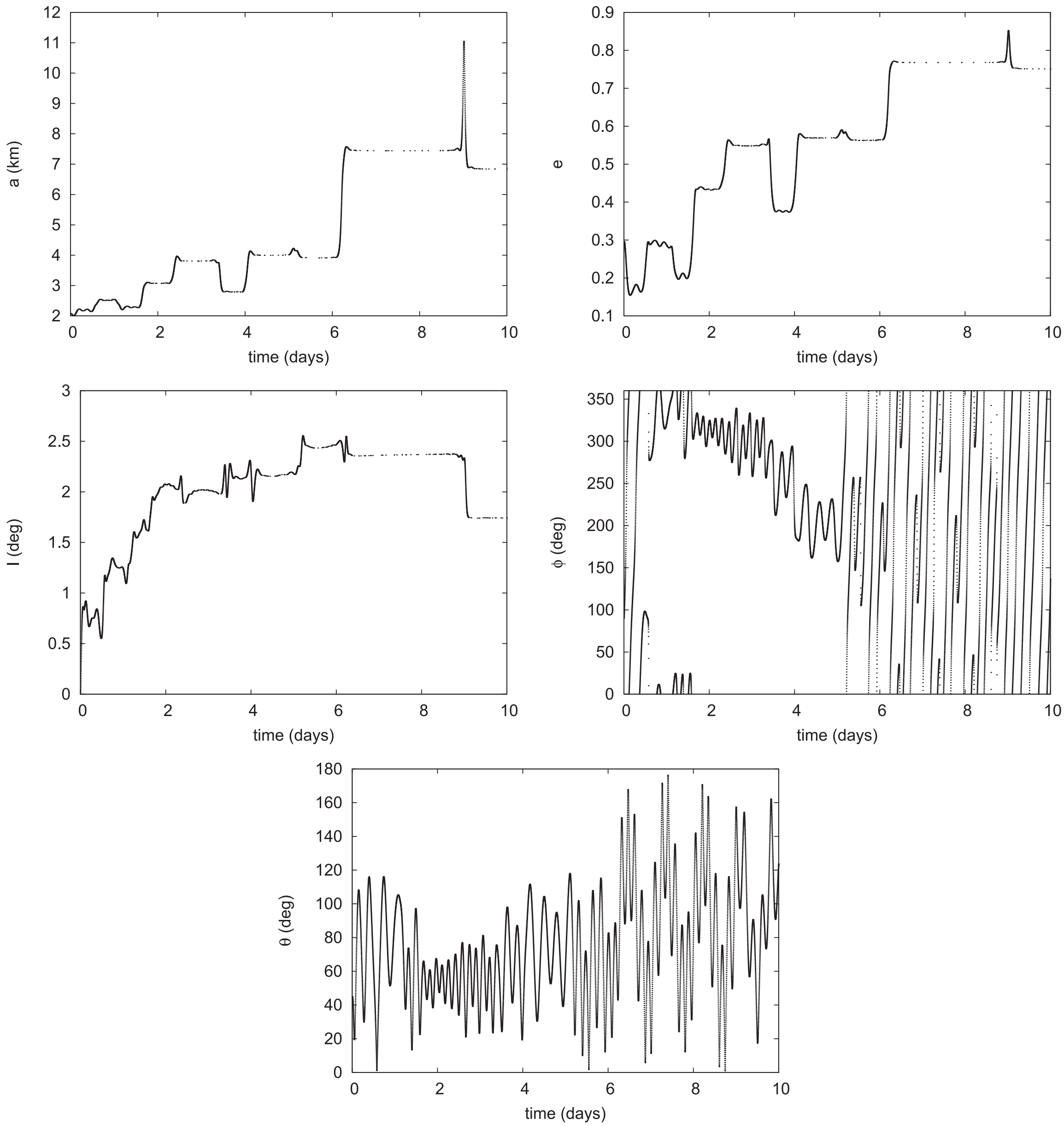

Figure 5. Orbit elements a, e and I, and Euler angles θ and ϕ of the secondary body as a function of time during 10 d. The initial obliquity is $\theta = 45^{\mathrm{o}}$ and the mass ratio is $q = 0.1$. Analysing the orbital elements and the Euler angles we can conclude that the orbital and rotational (nutation and precession) motion show a complex behaviour.

3.2 Initial conditions

We need many initial parameters to perform the simulations. The parameters are initial position and velocity of the secondary body (r_x, r_y, r_z, v_x, v_y, v_z), and spin velocity (w'_x, w'_y, w'_z), dimensions, mass and the initial orientation (Euler angles) of each body. We fixed the dimensions of the central body ($a_{(c)} = 1$ km, $b_{(c)} = 0.7$ km, $c_{(c)} = 0.65$ km) and the density ($d = 2.0$ g cm^{-3}), that we consider good values compared with previous works (Pravec et al. 2010; Jacobson & Scheeres 2011). We used 19 different values of mass ratio ($q_1 = 0.01, q_2 = 0.05, q_3 = 0.1, q_4 = 0.15, q_5 = 0.16, q_6 = 0.17, q_7 = 0.18, q_8 = 0.19, q_9 = 0.20, q_{10} = 0.21, q_{11} = 0.22, q_{12} = 0.23, q_{13} = 0.24, q_{14} = 0.25, q_{15} = 0.26, q_{16} = 0.27, q_{17} = 0.28, q_{18} = 0.29$ and $q_{19} = 0.30$). For the dimensions of the secondary body we use the relations $a_{(s)} = q^{1/3} a_{(c)}$, $b_{(s)} = q^{1/3} b_{(c)}$ and $c_{(s)} = q^{1/3} c_{(c)}$. The initial spin velocity we use is $\boldsymbol{\omega} = (0, 0, \omega_0)$, where ω_0 is the equilibrium rotation rate that we can compute using that relation (Scheeres 2009):

$$\omega_0 = \left[\frac{\mu}{r^3}\left[1 + \frac{3}{2r^2}\left[\frac{1}{M_{(c)}} Tr(\boldsymbol{I}_{(c)}) + \frac{1}{M_{(s)}} Tr(\boldsymbol{I}_{(s)}) - 3\left(A_{(c)} + A_{(s)}\right)\right]\right]\right]^{1/2}, \tag{9}$$

where $\boldsymbol{I}_{(i)}$ is the inertia dyads of these bodies. Finally, the spin velocity in the PAI system is $\boldsymbol{\omega}'_{\mathrm{i}} = T_{\mathrm{i}} \boldsymbol{\omega}$. The initial position of the secondary body is $\boldsymbol{r} = (r_0, 0, 0)$, where $r_0 = (a_{(c)} + a_{(s)} + 1 \times 10^{-5})$ km (1 cm of distance between the surfaces in the planar case), and the initial velocity is $\boldsymbol{v} = \boldsymbol{\omega} \times \boldsymbol{r}$. For every mass ratio we considered 91

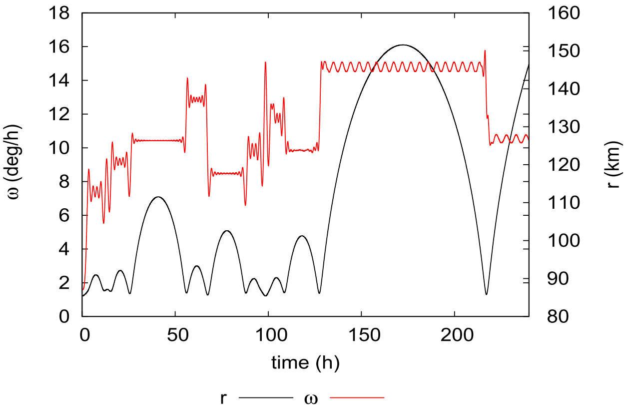

Figure 6. The modulus of spin velocity (ω) and the modulus of position vector as a function of time. Note the spin velocity changes abruptly when the bodies are close to each other.

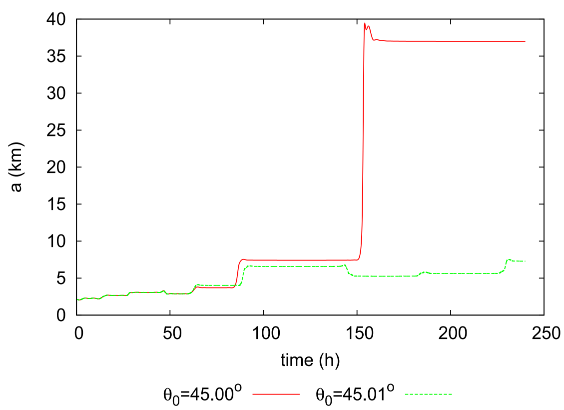

Figure 7. Temporal evolution of the semimajor axis for two different initial values Euler angle θ [$\theta_0 = 45\overset{\circ}{.}00$ (red) and $\theta_0 = 45\overset{\circ}{.}01$ (green)]. It shows the chaotic behaviour of the system, the two behaviours diverge strongly just after a few days.

different values of the inclination of the equator (Euler angle θ) for the secondary body $\theta_{(s)} = 0\overset{\circ}{.}0001, 1^\circ, 2^\circ, 3^\circ, \ldots, 90^\circ$ (see Fig. 4).

3.3 Conservation of angular momentum and energy

Knowing that the total energy and the total angular momentum of the system have to be conserved and in order to be sure of the validity of our simulations, we made some tests computing the total energy and total angular momentum of the system. The results showed that the quantities were conserved with relative error of the order for 10^{-11} for energy and 10^{-12} for angular momentum.

4 DYNAMICAL EVOLUTION

We first show some plots to illustrate the dynamical evolution of an example of our simulations. Fig. 5 shows the temporal evolution of the case with mass ratio 0.1 and initial obliquity of the secondary body equal to 45°. Note the complexity of the orbital and rotational dynamics of the system. This complexity occurs because the initial orbit starts in an unstable equilibrium configuration (Scheeres 2007), and the rotation motion is also in an unstable configuration, because the direction of the spin velocity does not coincide with an axis of principal inertial. This initial configuration occurs because the initial direction of the spin velocity is always in the same direction of the spin velocity before disruption (see Fig. 1). Because of that unstable initial condition, our simulations result in collision (when the bodies touch each other) or escape (when the secondary escapes from the central body), but the limit of simulation time is 200 yr, so for cases where the second body does not collide or escape until the end of the simulation are considered.

Fig. 6 shows the behaviour of the spin velocity of the secondary body during closer encounters with the central body. Note that the spin velocity changes abruptly during close approaches. The spin velocity can increase or decrease depending on the relative orientation of the bodies during the encounter (Scheeres et al. 2000).

The dynamical evolution of the system is also seen to be chaotic meaning that a small difference in initial conditions results in divergent outcomes. Fig. 7 shows the high sensitivity of the system to the initial inclination of the equator of the secondary body. It shows the evolution of the semimajor axis for two cases with a small difference of $0\overset{\circ}{.}01$ in the initial values of θ. Note that the two behaviours diverge strongly after just a few days.

5 EXTREME AND FINAL STATES

In this section we analyse the final and extreme states of our simulations. By final states we mean the state after the secondary body escapes or at the moment of collision, and the extreme states are the minimum or maximum values of a variable during the simulation. With these values we can obtain important information about the system such as the possibility of creation of a triple system.

To show examples of what kind of results that we can get, we made some plots of extreme and final states for three different mass ratios $q = 0.01$ (low value), $q = 0.15$ (medium value) and $q = 0.25$ (large value), for the 90 different values of θ_0. Figs 8–10 present the energy, the hyperbolic excess velocity (V_∞) for the escape cases, the final state of the spin period ($T_{\rm f}$), the lifetime ($t_{\rm l}$), final state of the orbital inclination ($I_{\rm f}$) and minimum spin period during the simulation ($T_{\rm min}$) for $q = 0.01$, 0.15 and 0.25, respectively. The spin period is computed by the magnitude of angular velocity ω: $T = 2\pi/\omega$; so that $T_{\rm min}$ is the minimum value of T during the simulation and $T_{\rm f}$ is the value of T at the end of simulation, that is after escape, at the moment of collision or after 200 yr (survive case). There are two lines (plots of $T_{\rm f}$ and $T_{\rm min}$) where one of them indicates the initial spin period ($T(t = 0)$) and the other is the spin period necessary for fission of the secondary body to occur (we call this limit period $T_{\rm r}$). So, the cases with $T_{\rm min} < T_{\rm r}$ indicate that secondary fission can occur. We can draw some general conclusions by comparing these three different systems. From Figs 8(a), 9(b) and 10(a) we see that the final lifetime $t_{\rm l}$ is directly proportional to the mass ratio of the system, in other words, $t_{\rm l}$ is larger for larger values of q. The variables $T_{\rm f}$ and $T_{\rm min}$ have the same behaviour as $t_{\rm l}$. To better figure out that general behaviour from our results, we made some plots of the average of a few of these variables with their respective standard deviation (Figs 11 and 12). In these figures it is easy to see that $\langle T_{\rm min}\rangle$, $\langle T_{\rm f}\rangle$, $\langle t_{\rm l}\rangle$ and $\langle I_{\rm f}\rangle$ are directly proportional, and $\langle V_\infty\rangle$ is inversely proportional to the mass ratio q. This means that the cases with large mass ratio have a longer lifetime, larger final inclination and less secondary spin fission than cases with low mass ratio. It is important to note that this general behaviour agrees with the planar case (Jacobson & Scheeres 2011).

To try to understand how the system evolution depends on the initial inclination of the equator θ_0, we choose four different values of θ_0: two extremes values ($0\overset{\circ}{.}0001$ and 90°) and two medium values

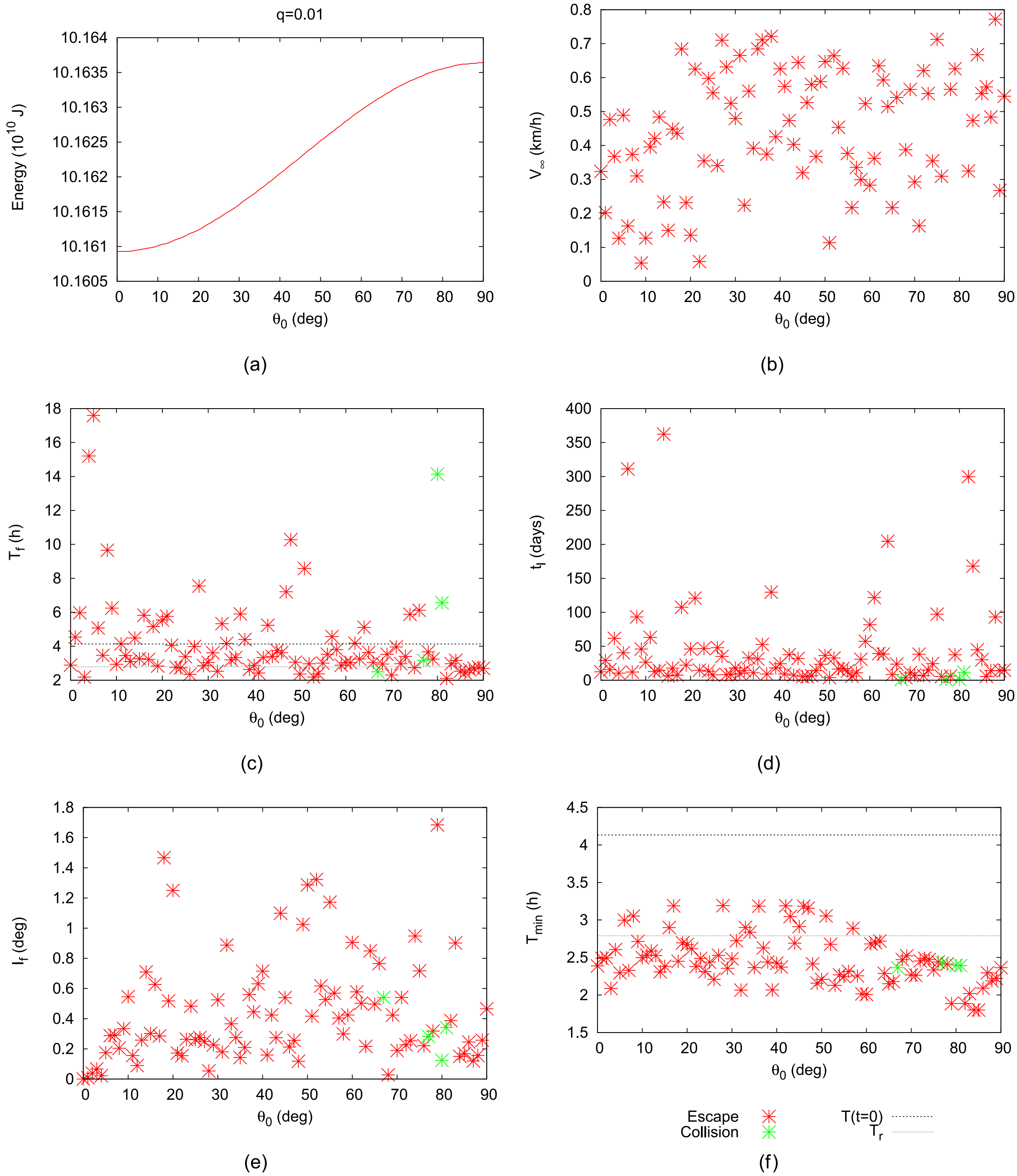

Figure 8. The final and extremes quantities of the second body as function of initial obliquity (θ_0) for the case with mass ratio $q = 0.01$. We present in this figure the total energy, the hyperbolic excess velocity (V_∞) for the escaping cases, the final secondary spin period (T_f), the lifetime (t_l), final state of the orbital inclination (I_f) and minimum secondary spin period during the simulation (T_{min}). Red denotes the cases where escape occurs and green are the cases where collision occurs. In the period plots there are two lines, the initial spin period ($T(t = 0)$) and the spin period necessary for fission of the second body (T_r), so the cases with T_{min} below T_r may go through another disruption. In this case ($q = 0.01$), 83 per cent of the cases experience secondary fission.

(30° and 60°). Then, we made simulations using a larger number of mass ratios q, shown in Fig. 13. Obviously, as shown before, these systems are chaotic, so we cannot take strong conclusions. We can conclude that I_f is larger in the medium values of θ_0 (blue and green lines), which can be explained due to exchange between spin and orbital angular momentum. We can also conclude similar behaviours in the T_{min} for all θ_0. If we consider the average behaviour, cases with $\theta_0 = 60^o$ tend to have a longer lifetime than other cases.

The collisions and secondary spin fission are important because these are situations that can lead the system to become a stable binary. It can be proven that planar systems started at fission conditions cannot re-impact (Scheeres 2009). However, the incorporation of non-planarity boosts the relative energy of the system and, at some point, enables impact to occur as another process. This distinguishes the current work from that of Jacobson & Scheeres (2011) which was conservatively just restricted to planar initial

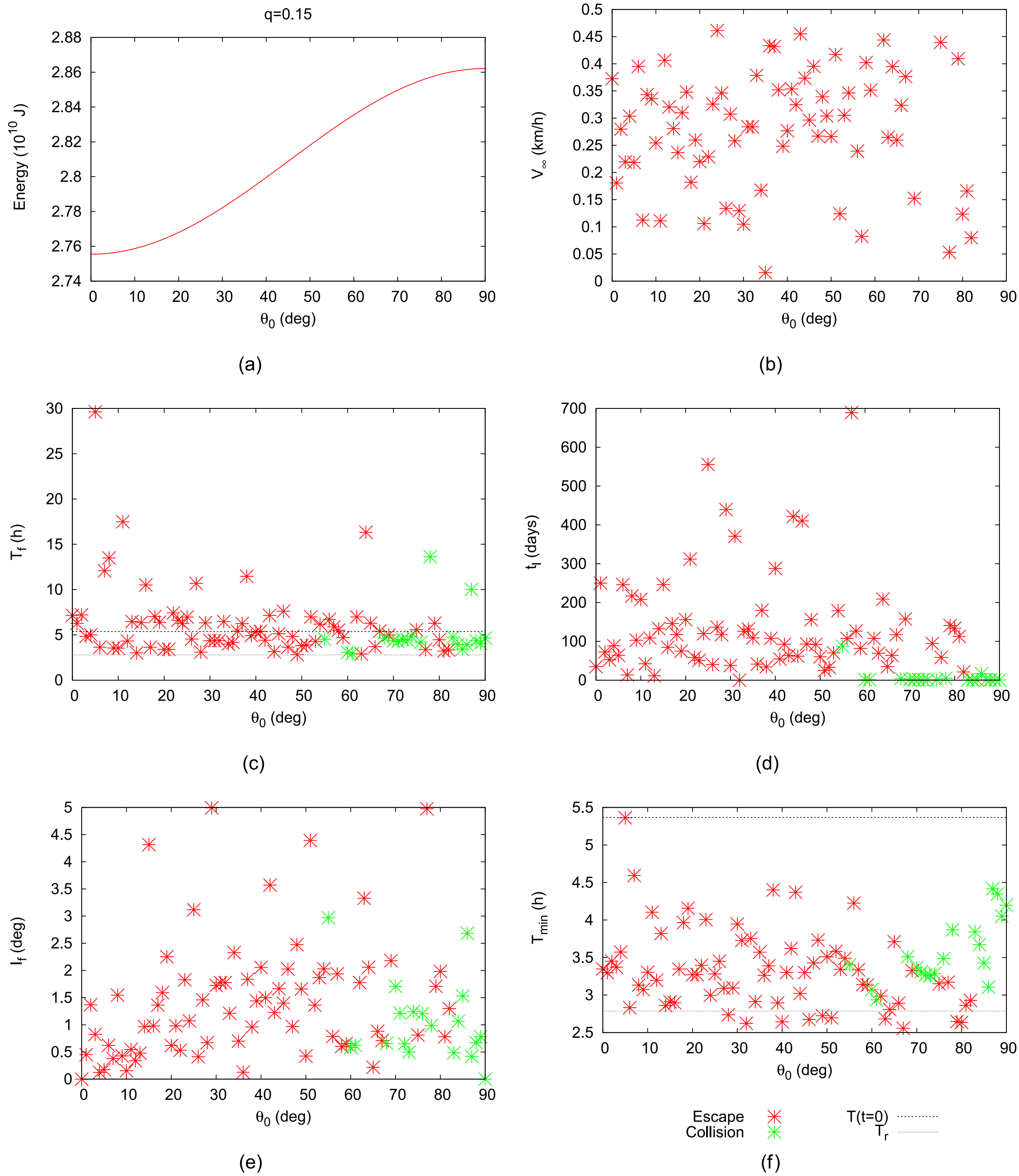

Figure 9. The final and extremes quantities of the second body as function of initial obliquity (θ_0) for the case with mass ratio $q = 0.15$. Plotted quantities are the same as in the previous figure. In this case ($q = 0.15$), 11.1 per cent experience secondary fission.

conditions. Figs 8–10 show that collisions generally only occur in cases with $\theta_0 \geq 50^o$ (however, note the collision with $\theta_0 = 40^o$ for $q = 0.17$), clearly related to the larger energy of these systems. This phenomenon also resembles the Lidov–Kozai mechanism (Kozai 1962; Lidov 1962), and deserves future study. We computed the frequency of cases which produced collisions and disruption of the secondary body and report these results in Table 1. Note, although it has small oscillations for large values of q, we can conclude the general behaviour that the percentage of collision is directly proportional and secondary disruption is inversely proportional to the mass ratio q. Collision cases, as said before, do not occur in planar cases, but in non-planar cases at least 4.4 per cent of the simulations ended in a collision. The case $q = 0.20$ has 32.2 per cent, almost one-third are collisions in this specific case.

We simulated 1260 different initial conditions and found that secondary fission should occur in 16 per cent of the cases and collisions in 22 per cent of cases. So, a significant part of the results are candidates to become a stable binary system.

Interesting results are the spin fission phenomena in cases with $q > 0.20$. The cases with $q > 0.20$ have at least a few percentage of secondary disruption. Jacobson & Scheeres (2011) did not find secondary spin fission in cases of $q > 0.20$ and their conclusion is

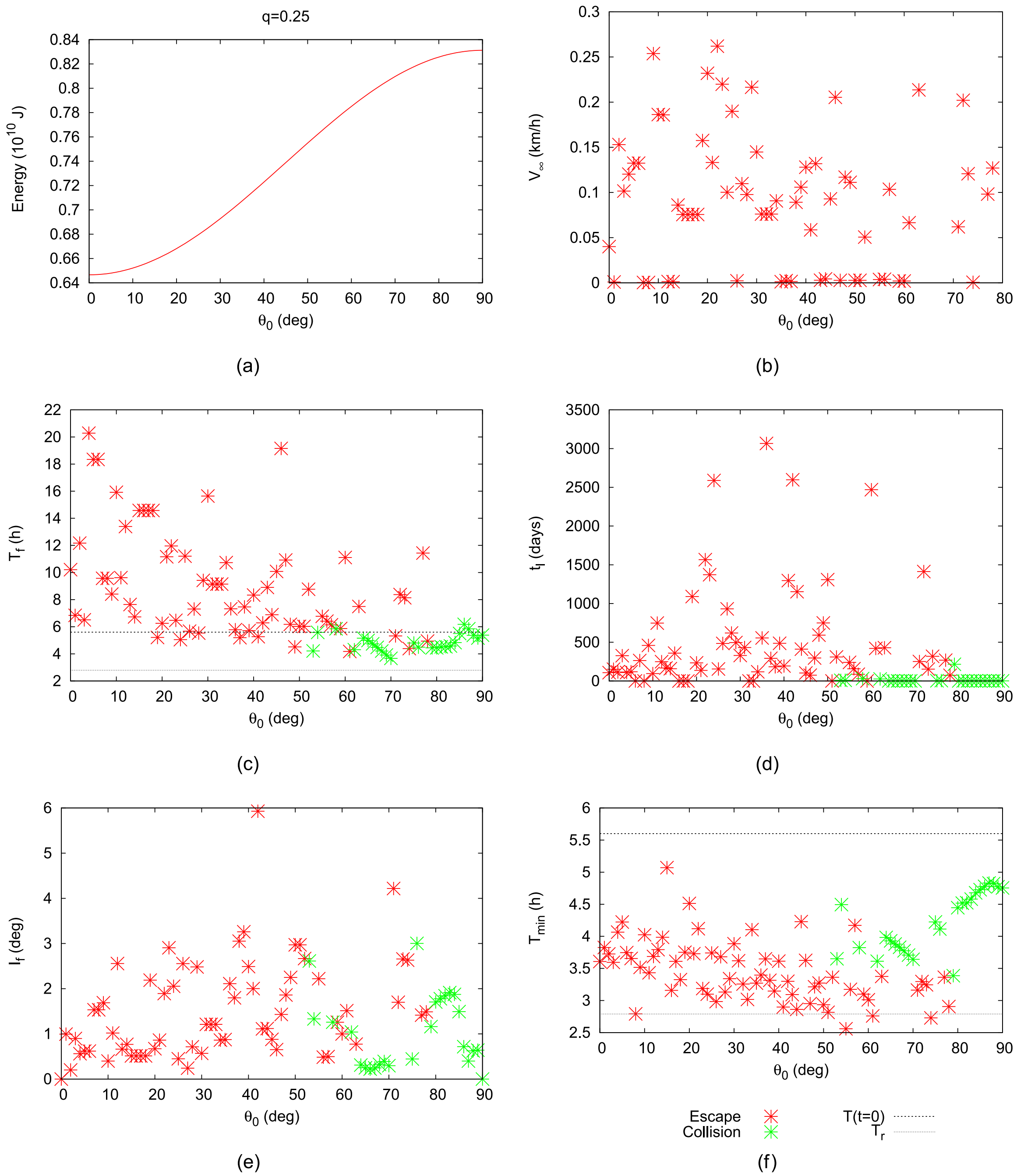

Figure 10. The final and extremes quantities of the second body as function of initial obliquity (θ_0) for the case with ratio of mass $q = 0.25$. Plotted quantities are the same as in the previous figures. In this case ($q = 0.25$), 4.4 per cent experience secondary fission.

that the chaotic systems with $q > 0.20$ can only become a stable binary through tidal process or BYORP process, but with our results we show that for the non-planar case this is not true. In other words, it is possible get a stable binary for $q > 0.20$ through a dynamical process (secondary disruption), but with low probability. It means that non-planar systems with large mass ratio can become a stable binary following the small ratio mechanisms outlined in Jacobson & Scheeres (2011), expanding this route to forming binaries.

We also analysed the rotational mode of the secondary characterized by the dynamic inertia I_D (Scheeres et al. 2000) for all escape cases, where $I_D = H^2/2E_k$, H is the magnitude of rotational angular momentum and E_k is the rotational kinetic energy. The parameter I_D tells whether the body is in a tumbling or non-tumbling state, and in the tumbling case whether it is in a long-axis mode (LAM) or short-axis mode (SAM). Uniform rotation (non-tumbling) can be about the largest moment of inertia $I_D = C$ or about the smallest moment of inertia $I_D = A$, and for all values of I_D between A and C the body is tumbling and will have precession and nutation. The condition for a body to be in a SAM rotation mode is ($B < I_D < C$), while the condition for it to be in an LAM rotation mode is ($A < I_D < B$). We choose nine equal regions between the values of A and C and computed the percentage of cases that the values of I_D finished in

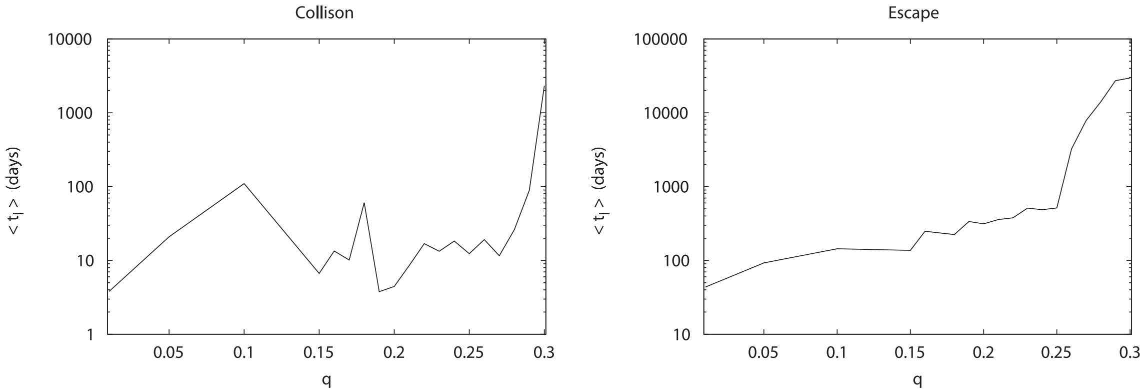

Figure 11. The average of lifetime ($\langle t_l \rangle$) as a function of the mass ratio q. The points are the average of the 90 initial obliquity values. On the right is the plot of the escape cases and on the left is the plot of the collision cases.

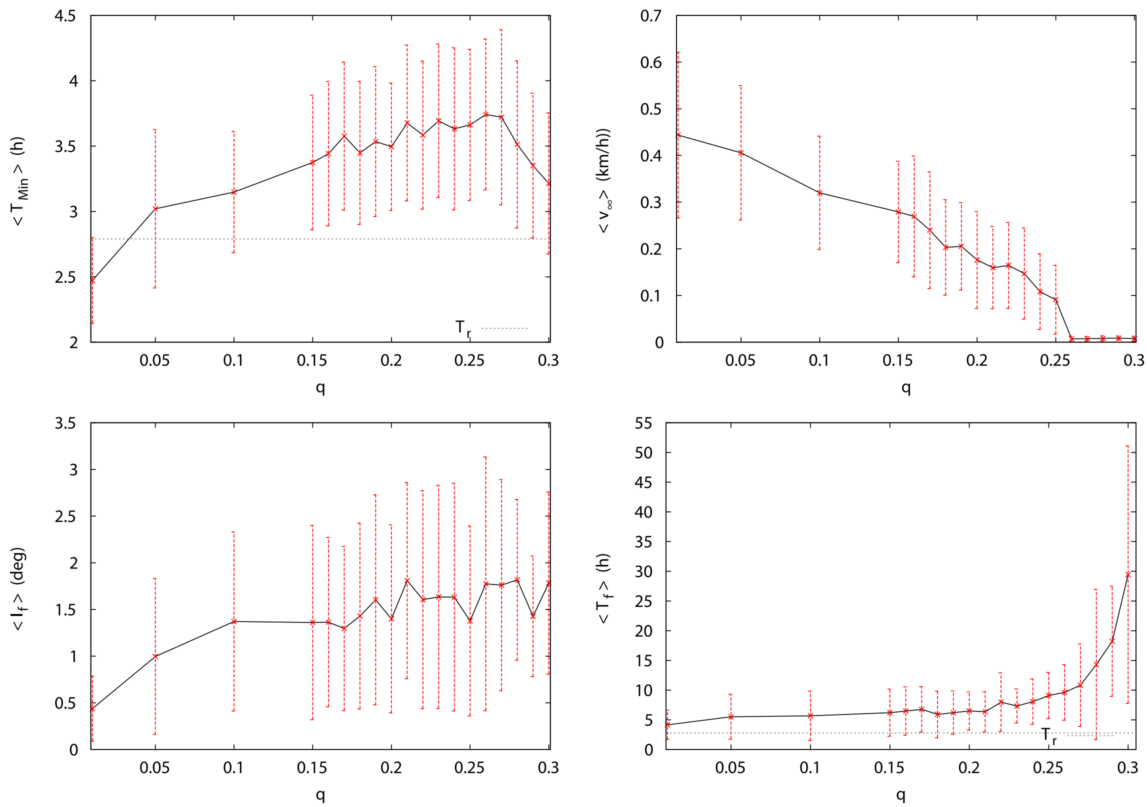

Figure 12. The averages of minimum spin period ($\langle T_{\min} \rangle$), final spin period ($\langle T_{\mathrm{f}} \rangle$) only for the escape cases, hyperbolic excess velocity ($\langle V_{\infty} \rangle$) and final state of the orbital inclination ($\langle I_{\mathrm{f}} \rangle$) as a function of the mass ratio q. The points are the average of the 90 initial obliquity values with their respective standard deviation (red bar).

each region, so we made a plot of these percentage of cases as a function of $I_{\mathrm{D}}^{\mathrm{f}}$ for all mass ratios studied, as shown in Fig. 14. We can conclude that all of the bodies are in some state of tumbling after escape. Most of them are in SAM, and are closer to uniform rotation about the maximum moment of inertia. The bodies between B and A are in a LAM, and will likely take longer to settle into the principal axis rotation. We note that the most probable state seems to be close to rotation about the intermediate axis, followed by a SAM state and followed by a LAM state. In contrast we find all of the primary body spin states to be in a SAM state, with small excitation.

6 DISCUSSIONS AND CONCLUSIONS

The results reported here extend the initial analysis in Jacobson & Scheeres (2011) to a more realistic set of initial conditions, testing the effect that initially non-planar orientations have on the dynamical outcome and evolution of the system. The Jacobson & Scheeres (2011) results separated into two regimes: a high mass ratio regime ($q > 0.2$) and a low mass ratio regime ($q < 0.2$); and they concluded that in the high mass ratio regime the processes of escape and secondary fission did not occur, leading to a different evolutionary path for these bodies.

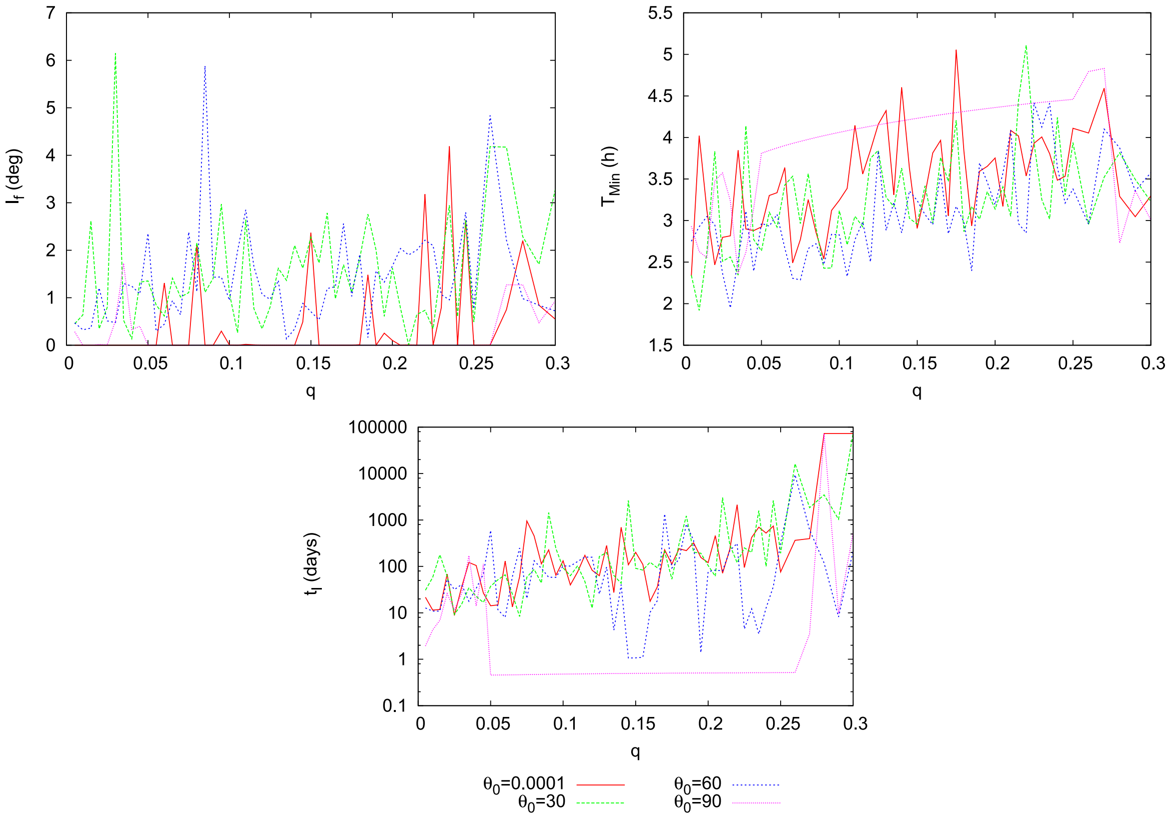

Figure 13. The final state of the orbital inclination ($I_{\rm f}$), minimum spin period ($T_{\rm min}$) and lifetime ($t_{\rm l}$) as a function of the mass ratio q for four different initial obliquities ($\theta_0 = 0.^\circ0001$, 30°, 60° and 90°). We use $t_{\rm l} = 200$ yr for the survivors cases.

Table 1. Percentage of collision, escape survivors and the cases of secondary disruption for every mass ratio q. This percentage is out of 90 different initial obliquity θ. Survivors mean cases that the lifetime is larger than 200 yr.

q	Secondary disruption (%)	Collision (%)	Escape (%)	Survivors (%)
0.01	83.5	4.4	95.6	0.0
0.05	44.0	13.3	86.7	0.0
0.10	25.5	21.1	78.9	0.0
0.15	11.1	21.1	78.9	0.0
0.16	8.8	24.4	75.6	0.0
0.17	5.5	28.8	71.2	0.0
0.18	8.8	22.2	77.8	0.0
0.19	5.5	23.3	76.7	0.0
0.20	4.4	32.2	67.8	0.0
0.21	6.6	31.9	68.1	0.0
0.22	5.5	25.5	74.5	0.0
0.23	2.2	27.7	72.3	0.0
0.24	4.4	28.8	71.2	0.0
0.25	4.4	27.7	72.3	0.0
0.26	1.1	31.9	68.1	0.0
0.27	3.3	29.7	68.1	2.2
0.28	12.1	28.6	60.4	11.0
0.29	7.7	33.0	27.5	39.5
0.30	15.4	26.3	7.7	66.0

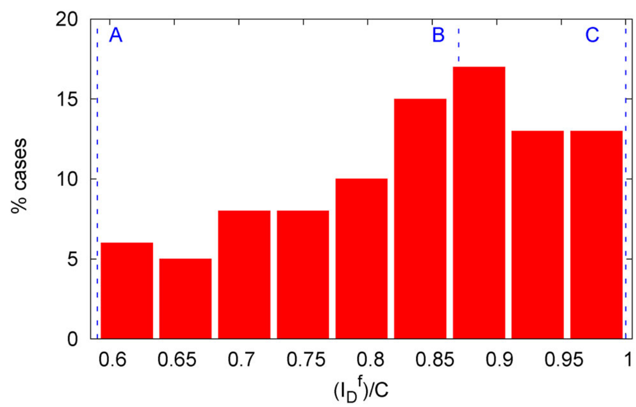

Figure 14. A bar graph of percentage cases as a function of $I_{\rm D}^{\rm f}/C$. The vertical lines are the values of A, B and C.

The introduction of an out-of-plane orientation of the secondary results in a relatively larger level of energy in the system for the same level of angular momentum. The theoretical implications of this is that the formerly found mass cut-off ratio should be relaxed, as a higher initial energy can both lead to escape in the system beyond the ideal planar limit (Scheeres 2009), and should also result in more secondary fission events at higher mass ratios. We note that the current model is, on average, more distended than those tested in the previous analysis (Jacobson & Scheeres 2011) and thus the low inclination cases cannot be directly compared. We do see a similar trend with mass ratio, seen in Fig. 12, where the number of secondaries going through secondary fission and the escape speeds of the escaping secondaries are both decreasing and heading to a point, at a higher mass ratio here, where they may disappear.

We also studied the rotation mode of the secondary body after disruption. The initial θ different from zero causes the body to start the simulation with initial state in tumbling mode, LAM or SAM. Analysing the value of final dynamic inertia $I_{\mathrm{D}}^{\mathrm{f}}$ of the secondary body we concluded that it tends to be close to rotation about the intermediate axis, followed by a SAM state and followed by a LAM state.

This is relevant for the results presented in Pravec et al. (2010), along with newer results shown in Scheeres et al. (2015). The original Pravec paper showed the sharp cut-off in asteroid pairs at the $q \sim 0.2$ mass ratio, as predicted from theory. More recent observations have shown a few bodies beyond this limit. Possible conclusions drawn from the current study is that most asteroid fission events involve less distended bodies, potentially closer to a planar initial configuration. The few outliers could be explained as more distended initial fissioned bodies or stronger non-planarity, which would result in the possibility of ejecting secondaries with a larger mass ratio – as is shown in the current study.

For future work we intend to analyse the dependence of the initial parameters of the central body (dimensions, density and direction of spin velocity) on the results, and the possible Lidov–Kozai mechanism in the collision cases. We also intend expand this study for cases with mass ratio larger than 0.30. Such a study could develop clearer understanding on how the morphology of the fissioned system relates to the range of possible outcomes.

ACKNOWLEDGEMENTS

The main author acknowledges the members of the Celestial and Spaceflight Mechanics Laboratory (CSML) and *Grupo de Dinâmica Orbital and Planetologia* that helped and advised us in this paper; Marcelo Wendling who helped us to make the illustrative figures; CAPES, FAPESP (proc. 2011/08171 − 3), PROPe-Unesp and CNPq for supporting this research. The authors are also grateful to Petr Pravec for all his suggestions.

REFERENCES

Beutler G., 2005, Methods of Celestial Mechanics. Vol. I: Physical, Mathematical, and Numerical Principles. Springer-Verlag, Berlin
Bottke W. F., Jr, Cellino A., Paolicchi P., Binzel R. P., 2002, in Bottke W. F., Jr, Cellino A., Paolicchi P., Binzel R. P., eds, Asteroids III. Univ. Arizona Press, Tucson, AZ, p. 3
Chapman C. R. et al., 1995, Nature, 374, 783
Jacobson S. A., Scheeres D. J., 2011, Icarus, 214, 161
Kozai Y., 1962, AJ, 67, 591
Lidov M. L., 1962, Planet. Space Sci., 9, 719
Margot J. L., Nolan M. C., Benner L. A. M., Ostro S. J., Jurgens R. F., Giorgini J. D., Slade M. A., Campbell D. B., 2002, Science, 296, 1445
Merline W. J., Weidenschilling S. J., Durda D. D., Margot J. L., Pravec P., Storrs A. D., 2002, in Bottke W. F., Jr, Cellino A., Paolicchi P., Binzel R. P., eds, Asteroids III. Univ. Arizona Press, Tucson, AZ, p. 289
Pravec P. et al., 2010, Nature, 466, 1085
Press W. H., Teukolsky S. A., Vetterling W. T., Flannery B. P., 2007, Numerical Recipes: The Art of Scientific Computing, 3rd edn. Cambridge Univ. Press, New York
Scheeres D. J., 2002, Icarus, 159, 271
Scheeres D. J., 2007, Icarus, 189, 370
Scheeres D. J., 2009, Celest. Mech. Dyn. Astron., 104, 103
Scheeres D. J., Ostro S. J., Werner R. A., Asphaug E., Hudson R. S., 2000, Icarus, 147, 106
Scheeres D. J., Brit D., Carry B., Holsapple K. A., 2015, in Michel P., DeMeo F. E., Bottke W. F., eds, Asteroids IV. Univ. Arizona Press, Tucson, AZ
Walsh K. J., Richardson D. C., 2006, BAAS, 38, 582
Walsh K. J., Richardson D. C., 2008, Icarus, 193, 553
Wertz J. R., ed., 1978, Astrophysics and Space Science Library, Vol. 73, Spacecraft Attitude Determination and Control. Reidel, Dordrecht

This paper has been typeset from a TEX/LATEX file prepared by the author.